ORIGINAL RESEARCH PAPER

Se doped ZnO nanoparticles with improved catalytic activity in degradation of Cholesterol

Bhavani Prasad Nenavathu[1]*, Aarti Sharma[2], Raj Kumar Dutta[3]

[1] *Department of Applied Sciences and Humanities, Indira Gandhi Delhi Technical University for Women, Delhi, 110006, India*

[2] *School of Technology Management and Engineering, SVKM's Narsee Monjee Institute of Management Studies, Navi Mumbai- 410210, India*

[3] *Department of Chemistry, Indian Institute of Technology, Roorkee-247667, India*

ABSTRACT

Pristine and Se doped ZnO nanoparticles (NPs) were successfully synthesized by the thermo-mechanical method and their structural, morphological and optical properties are characterized. Here in, a series of experiments were carried out where cholesterol is treated with the same concentration of Pristine as well as Se doped ZnO NPs. Several Cholesterol oxidation products (COP's) such as 25-hydroxycholesterol and 26-hydroxycholesterol, 7α-hydroxycholesterol, 7β-hydroxycholesterol, 7-ketocholesterol are formed as observed by HPLC analysis. The batch of 5 wt % Se doped ZnO NPs exhibited highest cholesterol degradation efficiency followed by pristine ZnO NPs and 2 wt % Se doped ZnO NPs. The peak area corresponding to 7-ketocholesterol and 25-hydroxycholesterol is found to be 200980 AU and 200986 AU respectively. The mechanism of cholesterol degradation was correlated with the incorporation of oxygen vacancies due to Se doping, which was likely intermediate levels for transiting photoexcited charge carriers for generation of hydroxyl radicals. Further, hydroxyl radicals generated during the interaction of ZnO nanoparticles with aqueous media have been determined using terephthallic acid assay and 2′, 7′-di-chlorofluorescein (DCF) assay.

Keywords: *Cholesterol, Food Safety, Reactive Oxygen Species, Selenium Doping, ZnO Nanoparticles*

INTRODUCTION

Nanotechnology introduced in the food packaging industry can potentially provide solutions to food packaging challenges such as short shelf life [1, 2]. A variety of nanomaterials like silver nanoparticle (Ag NP), nanoclay, nano-zinc oxide (nano-ZnO), nano-titanium dioxide (TiO$_2$), carbon nanotubes (CNTs), possess antimicrobial property and can withstand the thermal and mechanical stress during food processing, stability, transportation, and storage which rendered them to use in food packaging [3-9] and their higher photocatalytic activity could be used in degradation of toxic dye [10-13]. The nanoparticles

(NPs) improved the quality of food and packaging mainly by three mechanisms, via the release of antimicrobial ions, the formation of Reactive Oxygen Species (ROS) by the effect of light radiation and damaging the integrity of bacterial cell [14-17]. However, the final consumers of food, packaged with nanocomposite materials, may come across the toxic degraded products and the degraded products may be absorbed and accumulated within the body. Thus, the initial concern would be to verify the consequences of the interaction of NPs from the packaging material with several food products [18,19]. In this regard, ZnO NPs are more attractive compared to Ag NPs, owing to its less

* Corresponding Author Email: *bhavaniprasadnaik@igdtuw.ac.in*

toxicity, easy to fabricate, more affordable quality. Several ZnO NPs based food products already exist in the market. SongSing Nano Technology Co., Ltd. designed a plastic wrap containing nano-ZnO for food and beverage packaging [20]. The antibacterial activity of ZnO on *Salmonella typhimurium* and *Staphylococcus aureusin* in ready-to-eat poultry meat was investigated [21]. Also, the biocidal action of polyethylene coated nano-ZnO composite film against model bacteria *Escherichia coli* was tested [22]. It is reported that cholesterol in food products can undergo auto-oxidation as well as oxidation in the presence of reactive oxygen species (ROS), resulting in to formation of oxidized cholesterol derivatives and several oxysterol species that are toxic and cause carcinogenicity, atherosclerosis, rheumatoid arthritis, cytotoxicity, carcinogenesis, alterations in cell membrane properties, suppression of immune function, diabetes and degenerative diseases such as Parkinson's and Alzheimer's [23,24]. The levels of oxidized cholesterol derivatives using HPLC combined with ultraviolet (UV) and refractive index (RI) were measured [25-26]. However, the toxicological impact of ZnO NPs must be evaluated to determine the positive or negative effects on their usages against food safety.

In this section, we fabricated and characterized pristine, Se doped ZnO NPs and studied its ROS induced catalytic effect towards oxidation of cholesterol and determined the cholesterol oxidized products using HPLC. Selenium was chosen due to its suitable chemical property, ease of synthesis of Se doped ZnO NPs. Moreover, the high reduction potential of Se is thought to be a favorable condition for extracting photoexcited electrons from conduction band and hence can facilitate the generation of reactive oxygen species (ROS). Further, the amounts of hydroxyl radicals and ROS generated during the interaction of ZnO NPs with aqueous media have been determined using terephthallic acid assay and 2′, 7′-di-chlorofluorescein (DCF) Assay.

MATERIALS AND METHODS

Triton X-100 and Cholesterol were obtained from HIMEDIA Chemicals, India. Zinc acetate dihydrate (Zn (O$_2$CCH$_3$)$_2$ .2(H$_2$O) was procured from SRL Pvt. Ltd., India and selenium metal powder was obtained from SD Fine-Chemicals limited, India. Oxalic acid dihydrate (H$_2$C$_2$O$_4$.2H$_2$O) was purchased from Ranbaxy Laboratories

Ltd. India. Sodium sulfate is obtained from RFCL Limited, India. 2′, 7′-di-chlorofluorescein (DCF), 7-Ketocholesterol, 25-hydroxtycholesterol, commercial grade (bare) ZnO NPs (<100 nm in size, 99.99%), were procured from Sigma Aldrich, Germany. Terephthallic acid was obtained from HIMEDIA Chemicals, India. All the chemicals and solvents were used without further purification.

Synthesis of Se doped and Pristine ZnO NPs

In a typical synthesis of Se doped ZnO NPs, 5.48 g of zinc acetate dihydrate, 3.78 g of oxalic acid and required amount of selenium metal powder (2 wt% and 5 wt% of Zinc acetate dehydrate) were mixed and grinded in an agate mortar at room temperature for 20 min. For 2 wt% and 5 wt %, Se doped ZnO NPs synthesis 0.1 gm and 0.27 gm of Selenium metal powder are taken respectively. Initially, the smell of the acetic acid could be detected for about 10 min indicating near completion of the reaction to form ZnC$_2$O$_4$·2H$_2$O. The product was transferred to a quartz crucible and heated at 450 ℃ for 30 min in a muffle furnace fitted with a Proportional-Integral-Derivative (PID) controller to ensure stability in the temperature. The heating temperature was kept at 450 ℃ as the thermogravimetric analysis of the as obtained grinded ZnC$_2$O$_4$·2H$_2$O showed a mass loss at about 400 ℃, which suggested the formation of ZnO NPs and agreed well with our previously reported literature [27]. Similarly, a batch of ZnO NPs not doped with Se was prepared in the same manner as described above, except the addition of selenium metal. The NPs were washed with ethanol and kept for overnight drying at 60 ℃.

Characterization of Pristine and Se doped ZnO NPs

The X-ray diffraction measurements of the pristine and Se doped ZnO NPs were performed with powder diffractometer (Bruker ARS D8 Advance) operated at 40 kV using graphite monochromatized Cu K_α radiation source with a wavelength of 1.54 Å in a wide-angle region from 20° to 80° on a 2θ scale. The particle size distribution and morphology of pristine ZnO NPs and Se doped ZnO NPs were characterized using FESEM EDAX (Field emission scanning electron microscope coupled to energy dispersive X-ray analyzer), FEI-Quanta 200F operated at 20 kV. The sample for SEM measurements was prepared by spraying the dispersion of ZnO NPs on a clean glass plate, dried at room temperature and coated with a thin layer of Au. The TEM images were recorded using an FEI Technai-G^2 microscope operated at 200

290

J. Water Environ. Nanotechnol., 3(4): 289-300 Autumn 2018

kV and the corresponding elemental composition of the nanostructures was determined by the EDAX. The samples for TEM analysis were prepared by placing a drop of diluted Se (5 wt %) doped ZnO NPs dispersed on a carbon coated 150 mesh copper grid and dried at room temperature. The absorption spectrum of as-synthesized nanoparticles dispersion was measured by UV–visible spectrophotometer (Shimadzu, UV-1800) in the wavelength range of 200–800 nm. The emission spectra are recorded using fluorescence spectrophotometer (Shimadzu, RF-5301 PC) at the excitation wavelength (λ_{ex}) of 380 nm.

Measurement of •OH radicals using terephthallic acid assay

The batches of 0.6 mg/mL of pristine ZnO NPs and Se doped (2 wt % and 5 wt %) ZnO NPs were first sonicated for 10 min in 3 mM solution of terephthallic acid prepared in 0.01 M NaOH solution. The reaction mixture was then stirred continuously for 30 min to form adducts between •OH radicals and terephthallic acid. After stirring the reaction mixture was centrifuged at 7000 rpm for 5 min and emission spectrum of the supernatant was recorded using Shimadzu (RF-5301 PC) fluorescence spectrophotometer at the excitation wavelength (λ_{exc}) of 315 nm. A control experiment was carried out by measuring the intensity of the emission spectrum of the reaction mixture before UV illumination. The total number of •OH radicals generated during the course of the reaction was a measure of the fluorescence intensity of adducts formed between the •OH radical and terephthallic acid [28]. All analyses were performed in triplicate and the results are presented as mean and standard deviation of three analyses.

Measurement of ROS using Dichloro fluorescein di acetate assay (DCFDA assay)

The batches of 0.3 mg/mL of pristine ZnO NPs and Se doped (5 wt %) ZnO NPs were first sonicated for 10 min in 20 μM working solution of dichloro fluorescein di acetate prepared in water. The above reaction mixture was incubated by stirring in dark for one day. Then the reaction mixture was centrifuged at 7000 rpm for 5 min and the absorption spectrum was measured by UV–visible spectrophotometer (Shimadzu, UV-1800) in the range of 200–800 nm and similarly emission spectrum of the supernatant was recorded using Shimadzu (RF-5301 PC) fluorescence

spectrophotometer at excitation wavelength (λ_{exc}) of 296 nm. A control experiment was carried out where dye is untreated with NPs. The concentration of ROS generated during the course of the reaction was measured by observing the absorbance intensity and fluorescence intensity for the batches of 0.3 mg/mL of Pristine ZnO NPs and Se doped (5 wt %) ZnO NPs. All analyses were performed in triplicate and the results are presented as mean and standard deviation of three analysis.

Synthesis of 20 ppm of Cholesterol stock solution

Add 1 ml of Triton X-100 to a 500 mL wide-mouth Erlenmeyer flask and stirred continuously on a hot plate at temperature 50 °C. Add 20 mg of cholesterol to the 1 mL of Triton X-100 in Erlenmeyer flask and stir continuously at 50 °C till the whole cholesterol is dissolved. Do not allow the Triton X-100 to yellow or boil. Once the cholesterol is dissolved, add 250 mL of sterile double distilled water through the walls of flask slowly with continuous stirring. Do not allow the solution to become cloudy. Store the solution at 4 °C.

Degradation, extraction, and purification of Cholesterol Oxidation Products (COPs)

Pristine, Se doped ZnO NPs and commercial ZnO NPs were added to the test solution of 20 ppm concentration of cholesterol and stirred continuously for a period of 5 h. The reaction mixtures were ultrasonicated for 20 min in dark prior to the experiment to ensure uniform dispersion of the catalyst during the course of the reaction and for attaining proper adsorption-desorption equilibrium. The ZnO NPs, which act as a catalyst was removed from the reaction mixture by centrifuging at 5000 rpm for 5 min. The aliquot was then extracted with 10 mL chloroform. The organic layer was collected, dried with sodium sulfate, and evaporated using rotary evaporator (Yamato cold trap CA 300) to 0.5 mL volume. The concentrated organic extract was then diluted with 1 mL of ethanol. The decomposition of the cholesterol was compared with a control comprising of 20 ppm cholesterol solution, untreated with ZnO NPs (autoxidation). In addition, the cholesterol degradation efficiency of pristine and Se doped ZnO NPs was compared.

HPLC equipment and conditions

A Shimadzu (Tokyo, Japan) liquid chromatograph equipped with UV detector was used. The chromatographic conditions used in the present

J. Water Environ. Nanotechnol., 3(4): 289-300 Autumn 2018

291

study were as follows the analytical column used was a LiChrospher RP 18-e (HP) (5 μm, 250-4), injection volume 20 μL and oven temperature is 30 °C. The mobile phase for separation was acetonitrile and methanol (40:60, v/v) with a low-pressure gradient at a flow rate of 1 mL/min and an analysis time of 30 min. UV detection was performed with absorbance measured at two different wavelengths 205 nm and 234 nm. Cholesterol and Cholesterol oxidation products were identified by comparing retention times as well as peak area of samples with those of reference internal standards namely 7-ketocholesterol and 25-OH cholesterol.

RESULTS AND DISCUSSION

Characterization of as-synthesized Se doped ZnO NPs

The X-ray diffractogram of the as-synthesized Se doped (2 wt % and 5 wt %) ZnO NPs and Pristine ZnO NPs revealed characteristic peaks at (100), (101), (102), (110), (103) and (112) planes, corresponding to the hexagonal wurtzite phase of ZnO (JCPDS card No: 5–0664) [27]. As compared to pristine ZnO NPs, the XRD pattern of Se doped ZnO NPs revealed peak broadening and lowering in the intensity of the peaks. The peak broadening could be due to various reasons, namely, small particle sizes and strain due to defects in the nanomaterials [29]. The lowering in the intensity of the peaks could be attributed to decrease in the crystallinity of the ZnO phase due to Se doping. Notably, the intensity of the peaks decreased with increase in the atomic concentration of Se doping (Fig. 1). The crystallite sizes of the Se

doped ZnO NPs measured from Debye Scherrer formula [30] were less than the pristine ZnO NPs. The morphology of the Se doped ZnO NPs was revealed from SEM studies (Fig. 2a) and TEM studies (Fig. 2b). The average particle size of 5 wt % Se doped ZnO NPs was measured as 10.8 nm and corroborated well with the crystallite size derived from XRD measurement. The SAED pattern (shown in the inset Fig. 2b) indicates that all the ZnO nanoparticles are crystalline. The EDAX spectrum of the nanoparticles revealed characteristic X-ray peaks of Se and Zn, confirming the formation of Se doped ZnO nanoparticles (Fig. 2c). The peaks corresponding to Cu are due to the carbon-coated 150 mesh copper grids are used in sample preparation of TEM. Since ZnO is an n-type semiconductor, the increase in its band gap due to Se doping could be attributed to Burstein –Moss shift, which explains the shift in the absorption edge to higher energies due to merging of Fermi levels with the conduction band [31]. The increase in band gap of the Se doped ZnO NPs dispersed in aqueous medium was evident from the UV-visible absorption spectroscopy, where the λ_{max} corresponding to excitonic transition was measured at 359 nm and 360 nm for the batches of 2 wt % Se doped and 5 wt % Se doped ZnO NPs respectively, whereas λ_{max} for Pristine ZnO NPs it was 372 nm (Fig. 3a). Notably, the excitonic peak measured at 360 nm for the batch of 5 wt % Se doped ZnO NPs corresponded to 10.9 nm particle size, measured by using effective mass approximation method and this data agreed well with the corresponding crystallite size of 10.8 nm measured by XRD. The band gap of
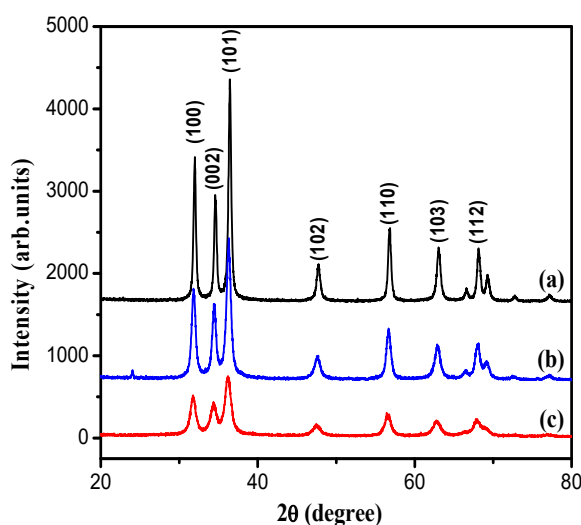

Fig. 1. XRD patterns of (a) Pristine ZnO NPs; (b) 2 wt % Se doped ZnO NPs; (c) 5 wt % Se doped ZnO NPs

292

J. Water Environ. Nanotechnol., 3(4): 289-300 Autumn 2018

Se doped ZnO NPs increased with the concentration of Se doping and was inversely correlated with the corresponding crystallite size as shown in Table 1. The low crystallite size of the catalyst possesses high surfaced area and induces high catalytic efficiency towards degradation of Cholesterol.

The emission spectroscopy of the dispersions of pristine and Se doped ZnO NPs was studied at the excitation wavelength (λ_{ex}) of 380 nm. In the case of pristine ZnO NPs, the emission peaks were recorded at 407 nm, 434 nm and at 460 nm (Fig. 3b). These near band edge (NBE) emission
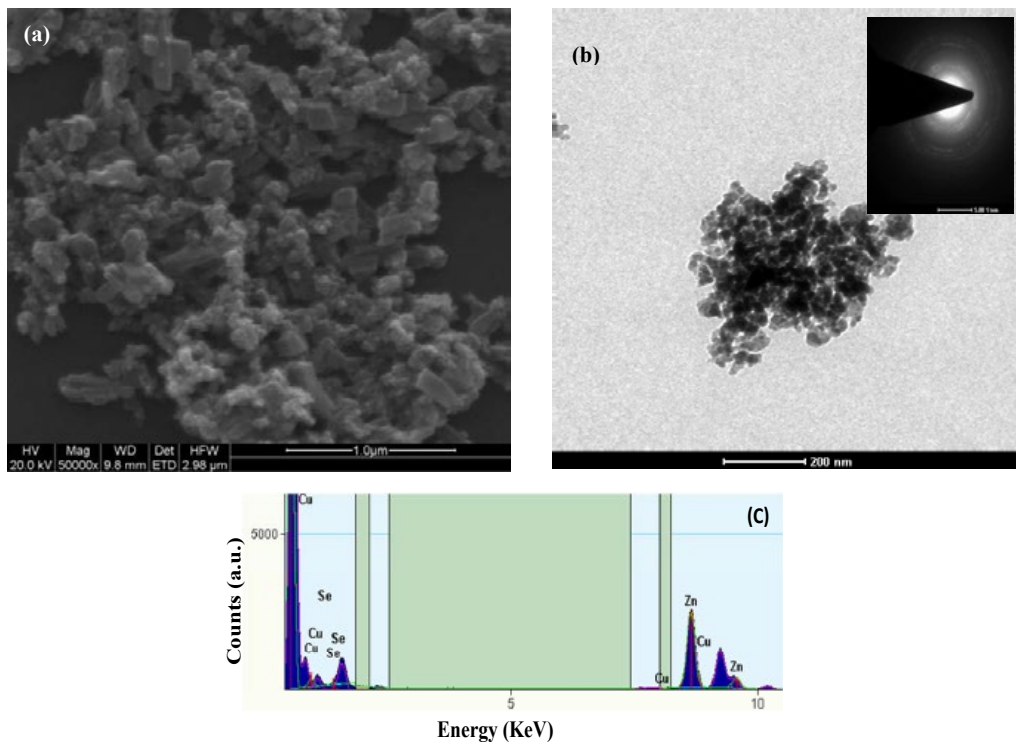

Fig. 2. Scanning electron microscopy of a representative nanostructure (a) 5 wt % Se doped ZnO NPs; (b) Transmission electron microscopy and inset showing the SAED pattern of 5 wt % Se doped ZnO NPs (c) energy dispersive X-ray analysis of a representative nanostructure of 5 wt % Se doped ZnO NPs.
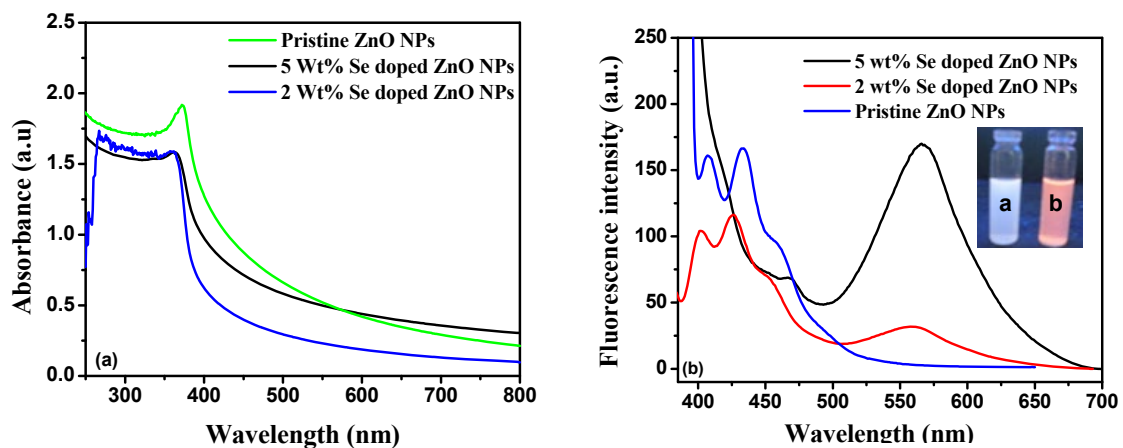

Fig. 3. (a) UV-visible absorption spectrum of Pristine ZnO NPs, 2 wt% Se doped ZnO NPs and 5 wt % Se doped ZnO NPs showing λ_{max} at 372 nm, 359 nm and 360 nm, respectively; (b) Fluorescence spectra of Pristine ZnO NPs, 2 wt% Se doped ZnO NPs and 5 wt % Se doped ZnO NPs using λ_{ex} = 380 nm. Inset (Marked b) showing pink coloured 5 wt % Se doped ZnO NPs

J. Water Environ. Nanotechnol., 3(4): 289-300 Autumn 2018

293

Table 1. Crystallite size (by XRD measurement) and band gap determined in pristine and Se doped ZnO NPs

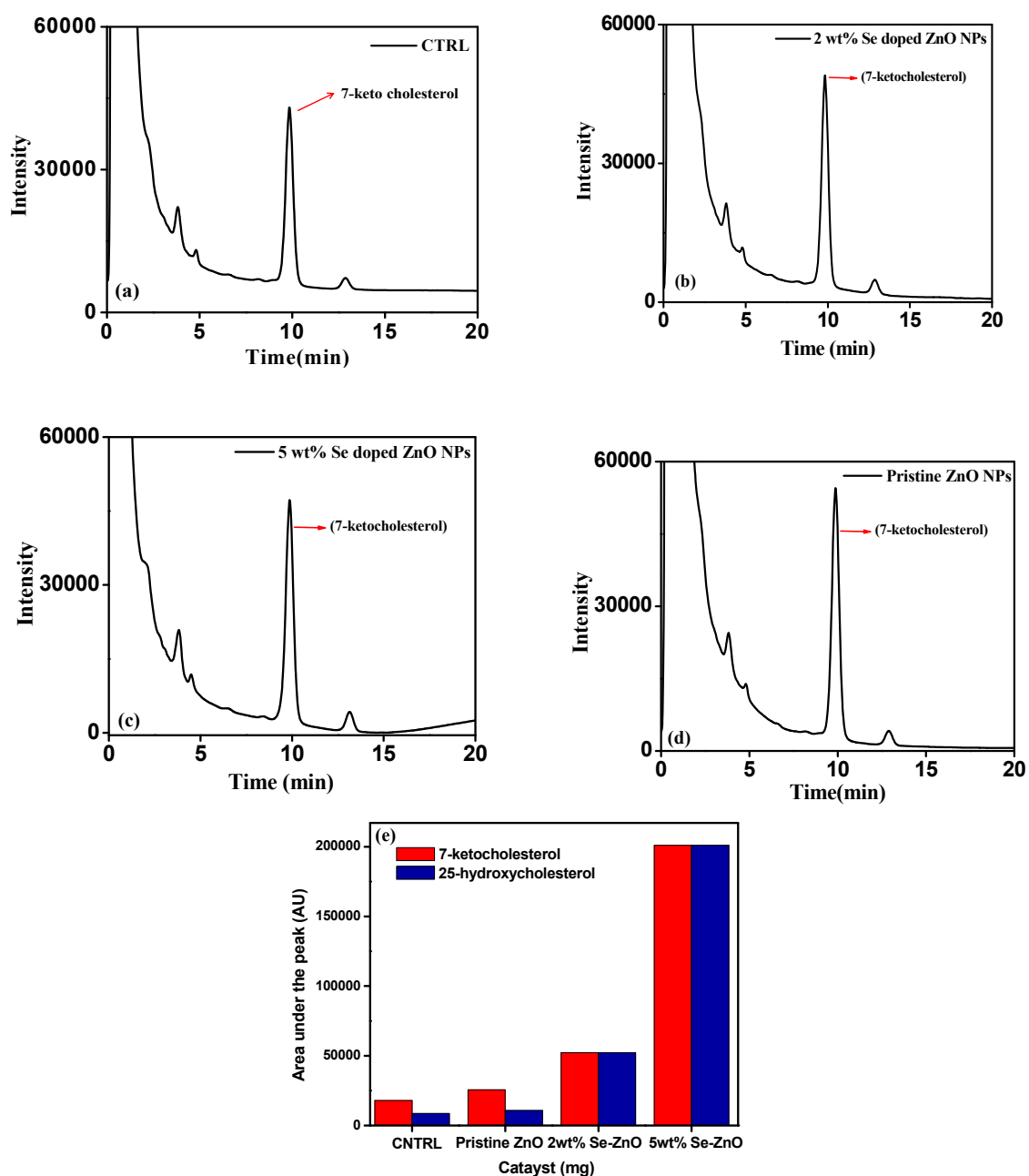| Photocatalyst	λmax (nm)	Crystallite size (nm)	Band gap (eV)
Pristine ZnO NPs	372	20.16	3.30
2 wt% Se doped ZnO NPs	359	14.0	3.50
5 wt% Se doped ZnO NPs	360	10.9	3.63

Fig 4. (a), (b), (c), (d) corresponds to the Chromatograms of cholesterol and cholesterol oxidation products obtained upon treatment of cholesterol with 2 wt %, 5 wt % and Pristine ZnO NPs determined using HPLC-UV. The numbered peaks correspond to (peak 1) 25-hydroxycholesterol, (peak 2) 26-hydroxycholesterol, (peak 3) 7α-hydroxycholesterol, (peak 4) 7β- hydroxyl cholesterol, (peak 5) 7-ketocholesterol. Fig.4. (e) shows the peak areas of 7-ketocholesterol and 25-hydroxycholesterol formed upon treatment of cholesterol with 5 wt % Se doped ZnO NPs, 2 wt % Se doped ZnO NPs, Pristine ZnO NPs

294

J. Water Environ. Nanotechnol., 3(4): 289-300 Autumn 2018

peaks at 407 nm and 434 nm corresponded to Zn vacancies and band to band transition, respectively [32]. On the other hand, the emission spectrum of the Se doped ZnO NPs revealed a reduction in the intensities of these NBE peaks and appearance of a new green emission peak at 565 nm. The intensity of the peak at 565 nm was appreciably high for the batch of 5 wt % Se doped ZnO NPs and notably, the NBE peaks for this batch were not recorded. Our results on the increase in the relative intensity of the green emission band with respect to the near band edge emission (NBE) band due to increase in the atomic concentration of Se dopant corroborated well with the reports of S doped ZnO nanostructures [33]. It may be remarked here that the broad green emission peak at 565 nm was due to surface oxygen vacancies [34]. A similar type of green emission peak due to oxygen vacancy was also reported for transition metal-doped TiO_2 NPs [35]. It is interesting to remark here that the aqueous dispersion of Se doped (5 wt %) ZnO NPs when viewed in a UV chamber excited by long wavelength (360 nm) appeared pink colored while the pristine ZnO NPs did not exhibit any color and is likely to corroborate oxygen vacancies in the doped NPs and the Se-doped ZnO NPs have very high concentrations of oxygen vacancies. The corresponding data is depicted in the inset Fig. 3b.

Mechanism of formation of Pristine and Se doped ZnO NPs

During the grinding process, solid particles of Zn $(CH_3COO)_2$ and $H_2C_2O_4 \cdot 2H_2O$ are in contact only at border points, so that surface atoms or molecules of $Zn(CH_3COO)_2$ and $H_2C_2O_4 \cdot 2H_2O$ react first. Because of this reaction enthalpy decreases, further reactions are initiated and sustained. Soon a barrier composed of the mixture of clusters of $ZnC_2O_4 \cdot 2H_2O$ and CH_3COOH in sizes ranging from tens of atoms to hundreds of atoms and in the form of particles, rods, thin flake and so on, is generated at points of contact of particles of $Zn(CH_3COO)_2$ and $H_2C_2O_4 \cdot 2H_2O$. This barrier prevents the unreacted $Zn(CH_3COO)_2$ and $H_2C_2O_4 \cdot 2H_2O$ from contacting directly so that the reaction is stopped. As the grinding process continues, the barrier is broken, and unreacted $Zn(CH_3COO)_2$ and $H_2C_2O_4 \cdot 2H_2O$ come into contact and react again. After the thermal decomposition of the ground powder mixture, $ZnC_2O_4 \cdot 2H_2O$ gives the formation of ZnO NPs. Since Selenium has a larger ionic radius than

oxygen, the incorporation of Selenium into the ZnO lattice will introduce lattice distortion. This effect influences the energy band structure of the ZnO NPs doped with Selenium, and as a result, new defects such as oxygen vacancies can be introduced by the new band structure deformation. Based on this reason, the green emission peaks are dominant peaks in the PL result of the as-grown Se-doped ZnO NPs.

Effect of Se doping concentration in degradation of cholesterol

A series of experiments were carried out where cholesterol is treated with the same concentration of pristine as well as Se doped ZnO NPs. The efficiencies of degradation of cholesterol for the batches of pristine ZnO NPs and the Se doped (2 wt % and 5 wt %) ZnO NPs was higher than the control batch (i.e., untreated cholesterol), as shown in Fig. 4. The peak areas of 7-ketocholesterol and 25-hydroxycholesterol formed upon treatment of cholesterol with 5 wt % Se doped ZnO NPs, 2 wt % Se doped ZnO NPs, Pristine ZnO NPs are shown in Fig. 4. (e). The intensity of the oxidation products of cholesterol was more for the batches treated with Se doped ZnO NPs than those treated with pristine ZnO NPs. Both the UV and RI detectors can be used to determine cholesterol and its oxidation products, herein UV was used because it is more sensitive and selective. The effect of catalyst concentration on the degradation of cholesterol was studied for a period of 5h. A control experiment is kept where cholesterol stock solution is analyzed immediately before auto-oxidation by HPLC. It was observed that the retention time of cholesterol is 25 min as shown in Fig. 5. After 5 h, the peak corresponding to cholesterol diminished and new peaks corresponding to cholesterol oxidation products are found. Fig. 4 shows the HPLC for cholesterol and its oxidative products using a reversed-phase column with UV detection at 210 nm. Cholesterol oxidation products (COP's) such as 25-hydroxycholesterol (Peak 1) and 26-hydroxycholesterol(Peak2),7α-hydroxycholesterol (peak 3), 7β-hydroxycholesterol (peak 4), 7-ketocholesterol (peak 5) showed absorbance at 210 nm whereas 7-ketocholesterol (Peak 5) showed absorbance both at 210 and 234 nm.

Table 2 shows the list of cholesterol oxidation products and their respective retention times. The peak areas of 7-ketocholesterol formed upon treatment of cholesterol with 5 wt % Se doped ZnO NPs, 2 wt % Se doped ZnO NPs, pristine ZnO
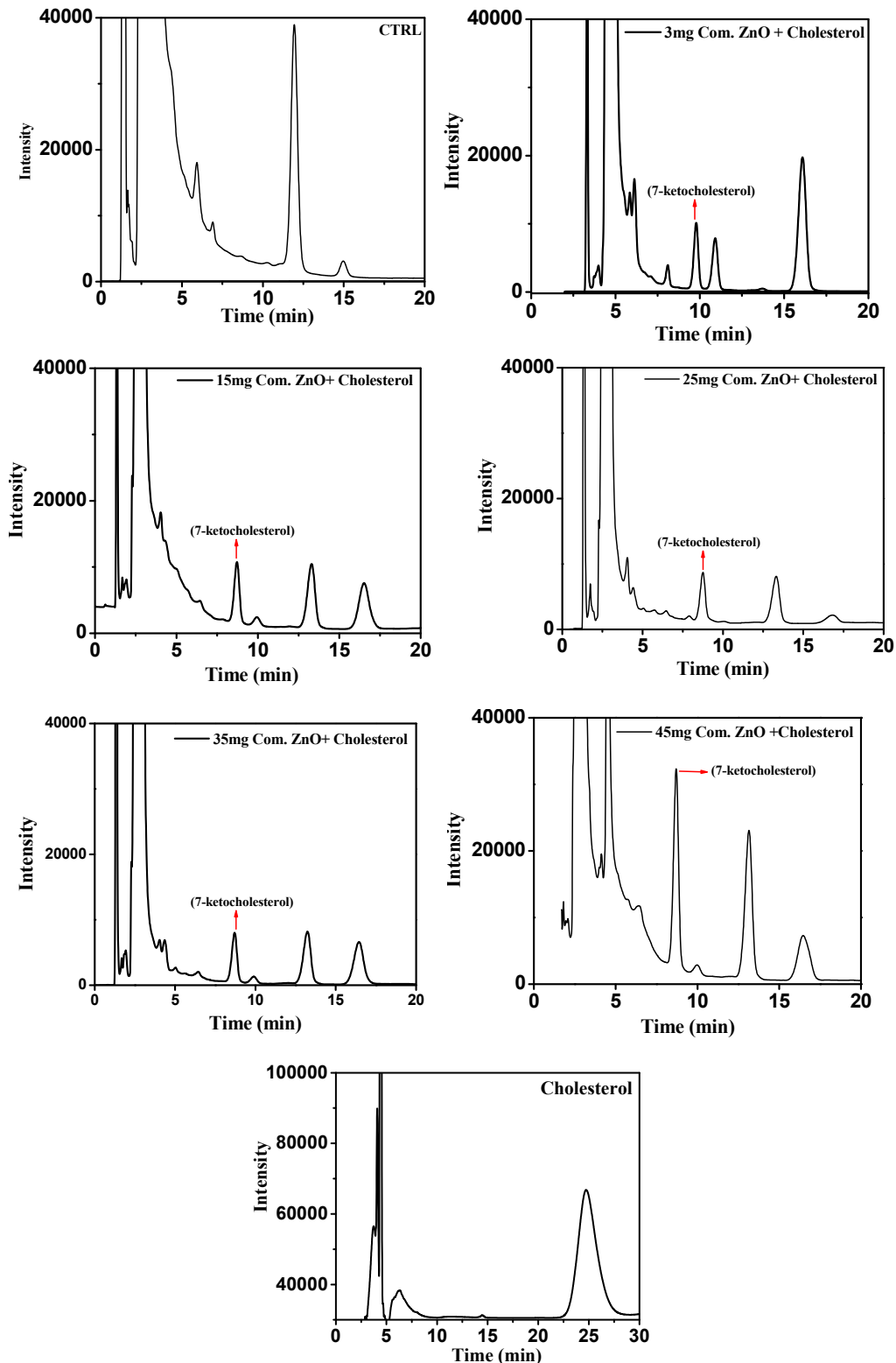
Fig. 5. Chromatograms of cholesterol and cholesterol oxidation products obtained upon treatment of cholesterol with commercial ZnO NPs of concentration varying (3,15,25,35,45 mg/40 mL) determined using HPLC-UV detected at 210 nm. The numbered peaks correspond to (peak 1) 25-hydroxycholesterol, (peak 2) 26-hydroxycholesterol, (peak 3) 7α-hydroxycholesterol, (peak 4) 7β-hydroxycholesterol, (peak 5) 7-ketocholesterol

296

J. Water Environ. Nanotechnol., 3(4): 289-300 Autumn 2018

NPs, and control are found to be 200980, 52226, 25606, 17940 AU respectively. The peak areas of 25-hydroxycholesterol formed upon treatment of cholesterol with 5 wt % Se doped ZnO NPs, 2 wt % Se doped ZnO NPs, Pristine ZnO NPs, and control are found to be 200986, 52226, 10751, 8658 AU respectively. From the peak areas, it is evident that the degradation efficiency of Se doped ZnO NPs is more than that of pristine ZnO NPs in degrading cholesterol. From Fig. 4 it is also clear that the auto-oxidation of cholesterol is completed in 5 h where no signs of cholesterol peak are being noticed.

Determination of cholesterol oxidation products (COPs)

Results obtained from quantification of oxysterols in different matrices have demonstrated that 7-ketocholesterol (7-KC) and 25-hydroxycholesterol (25-OH) are the most abundant COPs. Therefore, we decided to use 7-KC and 25-OH cholesterol as a tracer of cholesterol oxidation. Ultraviolet detection (UV) is the most commonly used method when cholesterol oxides are analyzed with HPLC. This detector is particularly useful for the analysis of COPs because these compounds show their maximum absorption at three wavelengths (≤210, 234, and 280 nm). In the case of cholesterol, a large diversity of oxides is formed, with their maximum UV absorption at different wavelengths. Hydroxycholesterols have their absorption maximum around 210 nm, 7-ketocholesterol at 233-245 nm and conjugated non-polar triens at 280 nm. There are also some cholesterol oxidation products such as 5α-epoxy cholesterol, 5β-epoxy cholesterol, and cholestanetriol that do not have double bonds and therefore have inadequate UV absorption.

Effect of commercial ZnO NPs (<100 nm in size) in degradation of cholesterol

Further, a series of experiments were carried out where cholesterol is treated with increasing concentrations of commercial ZnO NPs ranging 3, 8, 15, 25, 35, 45 mg /40 mL of solution and

the corresponding oxidation products formed were detected at 210 nm. The corresponding retention time of COPs is found to be 5.06, 6.5, 8.7, 9.9, 13.28, 16.51 min respectively. From the Fig. 5 it was observed that with an increase in the concentration of ZnO NPs the intensity of the peaks corresponding to the COPs has been increased. It has been observed that among these the most intense peak corresponded to 7-ketocholesterol at a retention time of 8.6 min. is noticed.

ROS induced catalytic effect by Pristine and Se doped ZnO NPs.

The electron-hole pairs (e^- h^+ pair) are produced due to absorption of light by ZnO NPs, which could either recombine or lead to production of highly active superoxide radical ($O_2^{\cdot -}$) due to electron mediated reduction of surface oxygen followed by formation of highly reactive oxygen species like hydroxyl radical (•OH) which act as primary oxidants for catalyzing degradation of cholesterol and organic compounds [36]. Similarly, the holes (h^+) can react with water to produce •OH radicals and cause degradation of cholesterol. Therefore, catalytic degradation requires suppression of e^- h^+ recombination. In our present study, this is achieved by Se doping in ZnO NPs that led to the formation of large concentrations of oxygen vacancies, as evident from the intense emission band at 565 nm which corresponded to 2.4 eV. This energy state appears in the forbidden gap of ZnO NPs (3.37 eV) and could facilitate interfacial electron (e^-) transfer to promote ROS generation.

Mechanism of degradation of Cholesterol

In general, •OH radicals are considered as principal ROS for enhanced degradation of the cholesterol [37]. Therefore, the degradation of cholesterol was likely to be due to the generation of hydroxyl radical during the interaction of pristine as well as Se doped ZnO NPs in the aqueous solution of the cholesterol. One may expect that both the C-4 and C-7 position of cholesterol should have an equal opportunity for an oxidative attack to

Table 2. Cholesterol and cholesterol oxidation products detected by using HPLC-UV detector and their corresponding retention times is also given

Peak no.	Compound name	Retention time
1	25-hydroxycholesterol	5.9
2	26-hydroxycholesterol	…
3	7α-hydroxycholesterol	…
4	7β- hydroxycholesterol	…
5	7-ketocholesterol	8.6

J. Water Environ. Nanotechnol., 3(4): 289-300 Autumn 2018
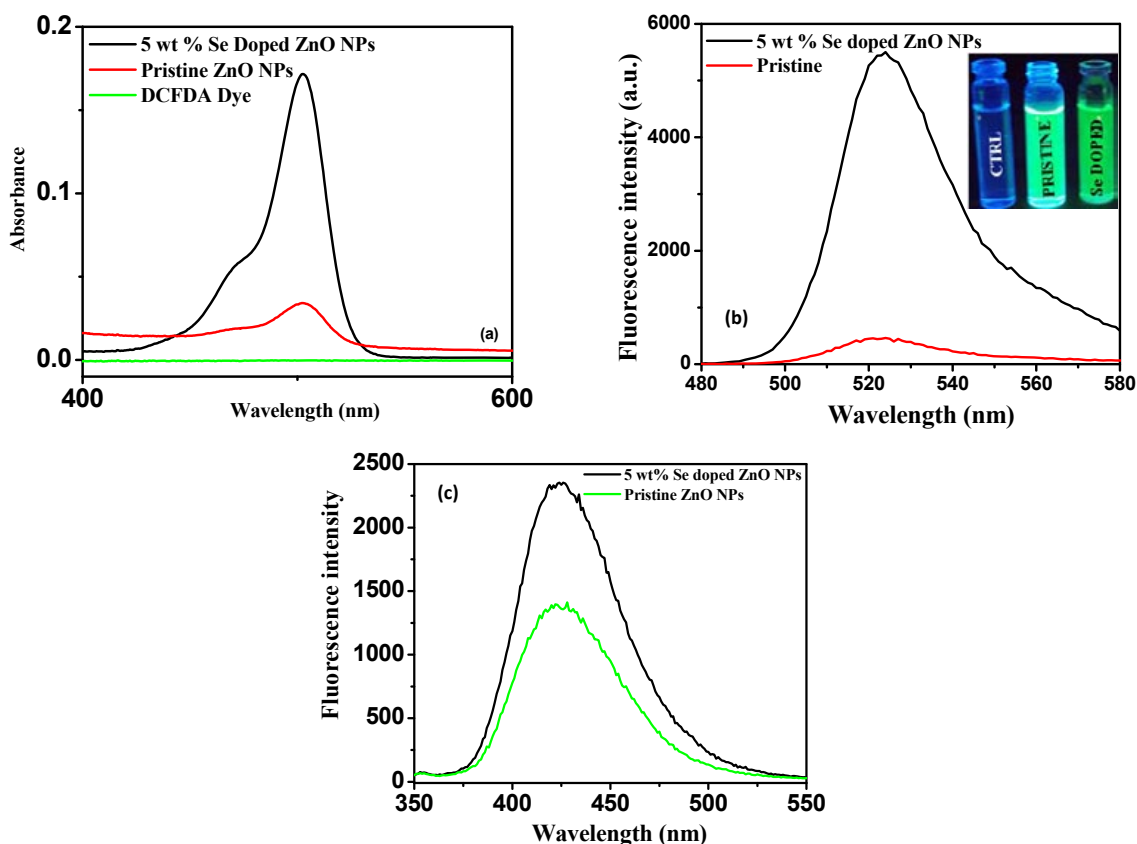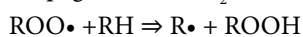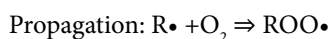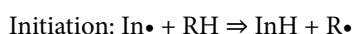
297

Fig. 6. (a) Absorbance and (b) fluorescence spectrophotometry of reduced and oxidized DCFDA dye (b) Inset showing green emission corresponded to oxidation of dye by Pristine and Se doped ZnO NPs (c) Fluorescence spectroscopy of terephthallic acid-OH radical adduct measured at excitation wavelength λ_{ex} = 315 nm for the batches of Se doped and Pristine ZnO NPs

occur. However, C-7 is indeed a common position for oxidants to react. In contrast, the attack rarely occurs at C-4 because of the possible shielding effect provided by the neighboring hydroxyl group at C-3 and the trialkyl substituted C-5 [38]. In addition, both the 20- C and 25-C of the aliphatic side chain are at a tertiary position, and are, more susceptible to oxidative attack than the other carbons [39]. Cholesterol oxidation by free radicals includes two types of reactions: the initiation and propagation reactions. Initiation is the first event in the lipid peroxidation process and is focused on a carbon with labile hydrogen: the carbon undergoes hydrogen abstraction followed by oxygen capture. These two initial reactions form a reactive species that further recruits non-oxidized lipids and start a chain reaction termed the propagation phase [40].

Initiation: $In\bullet + RH \Rightarrow InH + R\bullet$

Propagation: $R\bullet + O_2 \Rightarrow ROO\bullet$

$ROO\bullet + RH \Rightarrow R\bullet + ROOH$

Termination: $2ROO\bullet \Rightarrow$ non-radical products

Free radical autoxidation. In = initiator, R = lipid moiety • = radical.

Determination of ROS generation by Se doped ZnO NPs in aqueous media

In general, •OH radicals are considered as principal ROS for oxidation of the cholesterol [37]. Therefore, the degradation of cholesterol was likely to be due to the generation of hydroxyl radicals by the ZnO NPs in the aqueous solution. The generation of •OH radical was confirmed by the terephthallic acid assay [28]. The intensity of the fluorescent emission peak measured at λ_{max}= 425 nm corresponded to the formation of an adduct between the terephthallic acid and the •OH radicals formed due to the interaction of Se doped or pristine ZnO NPs in aqueous solution. The order of the intensities of the peak was 5 wt % Se doped > Pristine ZnO NPs, that correspond to the order of •OH radicals formed. Notably, the order

298

J. Water Environ. Nanotechnol., 3(4): 289-300 Autumn 2018

of intensities in Fig. 6c were the same as that of the oxidation efficiency. This indicated that the higher oxidation efficiency was due to higher •OH radical generation by the Se doped ZnO NPs, which acted as a catalyst. Similarly, 2', 7'-dichlorodihydrofluorescein diacetate (H_2DCFDA) is commonly used to detect the generation of reactive oxygen species. Non-fluorescent H_2DCFDA is converted to the highly fluorescent 2´,7´dichlorofluorescein (DCF) due to oxidation by ZnO NPs.

The oxidation of dye is being observed by noticing increase in absorbance at 286 nm and 502 nm and when this product is being excited at 296 nm the corresponding green emission is being recorded at 525 nm and the oxidation follows the sequence of Se doped ZnO NPs > pristine ZnO (Fig. 6a and 6b), which corresponds to the colour emission of reduced as wells as oxidised dye under short UV light.

CONCLUSIONS

Cholesterol is oxidized in the presence of reactive oxygen species generating aldehydes, hydroperoxides, and epoxides. It was possible to separate 6 species of oxidized cholesterol derivatives and cholesterol within 30 min using a reversed-phase column and methanol/acetonitrile (60:40, vol/vol) as the mobile phase at 1.0 mL/min with UV detection. The degradation efficiency of cholesterol was more for Se doped ZnO nanoparticles as compared to pristine ZnO nanoparticles. The mechanism of the degradation of cholesterol was discussed in the light of ROS generation during the interaction of catalyst in aqueous media. The role of ROS generation towards catalytic activity was proved by terephthallic acid assay and DCFDA assay. By comparing the ROS generation in pristine ZnO nanoparticles and Se doped ZnO nanoparticles, we could interpret the catalytic efficiency of the respective nanoparticles in the degradation of cholesterol. The doping by Se created large concentrations of oxygen vacancies, which were essential for restricting electron-hole pair recombination, and facilitated ROS generation for degradation of the cholesterol. Hence, the migration and exposure of nanomaterials from the food packaging to food consumer is to be monitored.

ACKNOWLEDGMENTS

SUPPLEMENTARY INFORMATION

Supplementary data to this article can be found online at http://www.jwent.net/

CONFLICT OF INTEREST

The authors declare that there are no conflicts of interest regarding the publication of this manuscript.

REFERENCES

1. Espitia PJP, Soares NdFF, Coimbra JSdR, de Andrade NJ, Cruz RS, Medeiros EAA. Zinc Oxide Nanoparticles: Synthesis, Antimicrobial Activity and Food Packaging Applications. Food and Bioprocess Technology. 2012;5(5):1447-64.
2. Handford CE, Dean M, Henchion M, Spence M, Elliott CT, Campbell K. Implications of nanotechnology for the agri-food industry: Opportunities, benefits and risks. Trends in Food Science & Technology. 2014;40(2):226-41.
3. Jin T, Sun D, Su JY, Zhang H, Sue HJ. Antimicrobial Efficacy of Zinc Oxide Quantum Dots againstListeria monocytogenes, SalmonellaEnteritidis, andEscherichia coliO157:H7. Journal of Food Science. 2009;74(1):M46-M52.
4. Sanchez-Garcia MD, Lagaron JM, Hoa SV. Effect of addition of carbon nanofibers and carbon nanotubes on properties of thermoplastic biopolymers. Composites Science and Technology. 2010;70(7):1095-105.
5. Applerot G, Perkas N, Amirian G, Girshevitz O, Gedanken A. Coating of glass with ZnO via ultrasonic irradiation and a study of its antibacterial properties. Applied Surface Science. 2009;256(3):S3-S8.
6. Sharma C, Dhiman R, Rokana N, Panwar H. Nanotechnology: An Untapped Resource for Food Packaging. Frontiers in Microbiology. 2017;8.
7. He X, Hwang H-M. Nanotechnology in food science: Functionality, applicability, and safety assessment. Journal of Food and Drug Analysis. 2016;24(4):671-81.
8. Bumbudsanpharoke N, Ko S. Nano-Food Packaging: An Overview of Market, Migration Research, and Safety Regulations. Journal of Food Science. 2015;80(5):R910-R23.
9. Szakal C, Roberts SM, Westerhoff P, Bartholomaeus A, Buck N, Illuminato I, et al. Measurement of Nanomaterials in Foods: Integrative Consideration of Challenges and Future Prospects. ACS Nano. 2014;8(4):3128-35.
10. Mohammadi, A. and A. K. Aliakbarzadeh, 2017. Methylene Blue Removal Using Surface-Modified TiO_2 Nanoparticles: A Comparative Study on Adsorption and Photocatalytic Degradation. Journal of Water and Environmental Nanotechnology, 2: 118-128.
11. Helmy, E. T., A. El Nemr, M. Mousa, E. Arafa and S. Eldafrawy, 2018. Photocatalytic degradation of organic dyes pollutants in the industrial textile wastewater by

J. Water Environ. Nanotechnol., 3(4): 289-300 Autumn 2018

299

using synthesized TiO$_2$, C-doped TiO$_2$, S-doped TiO$_2$ and C, S co-doped TiO$_2$ nanoparticles. Journal of Water and Environmental Nanotechnology, 3: 116-127.

12. Wang Y, Wang Q, Zhan X, Wang F, Safdar M, He J. Visible light driven type II heterostructures and their enhanced photocatalysis properties: a review. Nanoscale. 2013;5(18):8326.

13. Sharma A, Dutta RK. Se-doped CuO NPs/H 2 O 2 /UV as a highly efficient and sustainable photo-Fenton catalytic system for enhanced degradation of 4-bromophenol. Journal of Cleaner Production. 2018;185:464-75.

14. Fu PP, Xia Q, Hwang H-M, Ray PC, Yu H. Mechanisms of nanotoxicity: Generation of reactive oxygen species. Journal of Food and Drug Analysis. 2014;22(1):64-75.

15. Wang Y, Yuan L, Yao C, Ding L, Li C, Fang J, et al. A combined toxicity study of zinc oxide nanoparticles and vitamin C in food additives. Nanoscale. 2014;6(24):15333-42.

16. Pietroiusti A, Magrini A, Campagnolo L. New frontiers in nanotoxicology: Gut microbiota/microbiome-mediated effects of engineered nanomaterials. Toxicology and Applied Pharmacology. 2016;299:90-5.

17. Ray PC, Yu H, Fu PP. Toxicity and Environmental Risks of Nanomaterials: Challenges and Future Needs. Journal of Environmental Science and Health, Part C. 2009;27(1):1-35.

18. McClements DJ, Xiao H. Is nano safe in foods? Establishing the factors impacting the gastrointestinal fate and toxicity of organic and inorganic food-grade nanoparticles. npj Science of Food. 2017;1(1).

19. Chaudhry Q, Scotter M, Blackburn J, Ross B, Boxall A, Castle L, et al. Applications and implications of nanotechnologies for the food sector. Food Additives & Contaminants: Part A. 2008;25(3):241-58.

20. Tsuzuki T. Nanotechnology Commercialization. Pan Stanford Publishing; 2013.

21. Akbar A, Anal AK. Zinc oxide nanoparticles loaded active packaging, a challenge study against Salmonella typhimurium and Staphylococcus aureus in ready-to-eat poultry meat. Food Control. 2014;38:88-95.

22. Tankhiwale R, Bajpai SK. Preparation, characterization and antibacterial applications of ZnO-nanoparticles coated polyethylene films for food packaging. Colloids and Surfaces B: Biointerfaces. 2012;90:16-20.

23. Maerker G, Unruh J. Cholesterol oxides I. Isolation and determination of some cholesterol oxidation products. Journal of the American Oil Chemists' Society. 1986;63(6):767-71.

24. Korytowski W, Geiger PG, Girotti AW. Enzymatic Reducibility in Relation to Cytotoxicity for Various Cholesterol Hydroperoxides†. Biochemistry. 1996;35(26):8670-9.

25. Teresa Rodriguez-Estradaa M, Fiorenza Cabonib M. Determination of Cholesterol Oxidation Products by High-Performance Liquid Chromatography. Cholesterol and Phytosterol Oxidation Products: AOCS Publishing; 2002.

26. B.H C, Y.C C. Evaluation of the analysis of cholesterol oxides by liquid chromatography. Journal of Chromatography A. 1994;661(1-2):127-36.

27. Nenavathu BP, Krishna Rao AVR, Goyal A, Kapoor A, Dutta RK. Synthesis, characterization and enhanced photocatalytic degradation efficiency of Se doped ZnO nanoparticles using trypan blue as a model dye. Applied Catalysis A: General. 2013;459:106-13.

28. Hamal DB, Klabunde KJ. Valence State and Catalytic Role of Cobalt Ions in Cobalt TiO2 Nanoparticle Photocatalysts for Acetaldehyde Degradation under Visible Light. The Journal of Physical Chemistry C. 2011;115(35):17359-67.

29. Khorsand Zak A, Abd. Majid WH, Abrishami ME, Yousefi R. X-ray analysis of ZnO nanoparticles by Williamson–Hall and size–strain plot methods. Solid State Sciences. 2011;13(1):251-6.

30. Woo BK, Chen W, Joly AG, Sammynaiken R. The Effects of Aging on the Luminescence of PEG-Coated Water-Soluble ZnO Nanoparticle Solutions. The Journal of Physical Chemistry C. 2008;112(37):14292-6.

31. Bennett BR, Soref RA, Del Alamo JA. Carrier-induced change in refractive index of InP, GaAs and InGaAsP. IEEE Journal of Quantum Electronics. 1990;26(1):113-22.

32. Singh AK, Viswanath V, Janu VC. Synthesis, effect of capping agents, structural, optical and photoluminescence properties of ZnO nanoparticles. Journal of Luminescence. 2009;129(8):874-8.

33. Shen G, Cho JH, Yoo JK, Yi G-C, Lee CJ. Synthesis and Optical Properties of S-Doped ZnO Nanostructures: Nanonails and Nanowires. The Journal of Physical Chemistry B. 2005;109(12):5491-6.

34. Yalçın Y, Kılıç M, Çınar Z. Fe+3-doped TiO2: A combined experimental and computational approach to the evaluation of visible light activity. Applied Catalysis B: Environmental. 2010;99(3-4):469-77.

35. Khan H, Swati IK. Fe3+-doped Anatase TiO2 with d–d Transition, Oxygen Vacancies and Ti3+ Centers: Synthesis, Characterization, UV–vis Photocatalytic and Mechanistic Studies. Industrial & Engineering Chemistry Research. 2016;55(23):6619-33.

36. Iuliano L. Pathways of cholesterol oxidation via non-enzymatic mechanisms. Chemistry and Physics of Lipids. 2011;164(6):457-68.

37. Ansari GAS, Smith LL. THE OXIDATION OF CHOLESTEROL BY HYDROXYL RADICAL. Photochemistry and Photobiology. 1979;30(1):147-50.

38. Maerker G. Cholesterol autoxidation-current status. Journal of the American Oil Chemists' Society. 1987;64(3):388-92.

39. Smith, L. L. 1981. *Cholesterol Autoxidation*. Plenum Press, New York, U.S.A.

40. Niki E. Lipid peroxidation: Physiological levels and dual biological effects. Free Radical Biology and Medicine. 2009;47(5):469-84.

300

J. Water Environ. Nanotechnol., 3(4): 289-300 Autumn 2018